

## Article

# Geochemical Characteristics and Geological Significance of the Shangsü Mafic Dikes in Jiangxi

Yang Huang <sup>1,\*</sup>, Xinyue Chen <sup>1,\*</sup> and Yujiang Xie <sup>2</sup>

<sup>1</sup> School of Earth Science and Spatial Information Engineering, Hunan University of Science and Technology, Xiangtan 411101, China

<sup>2</sup> Jiangxi Fourth Geological Brigade, Pingxiang 337000, China; xieyujiang345@163.com

\* Correspondence: 21010103011@mail.hnust.edu.cn (Y.H.); chenxinyue@hnust.edu.cn (X.C.); Tel.: +86-159-7320-3098 (X.C.)

**Abstract:** Mafic dikes are developed in the Shangsü region of Jiangxi, including Nanyuan Mountain and Mianhuaao. These dikes intrude into the Upper Triassic Anyuan Formation and are primarily composed of pyroxene, plagioclase, and opaque minerals, exhibiting a dolerite texture. The mafic dikes were found to have an SiO<sub>2</sub> content ranging from 48.38% to 50.53% and the (K<sub>2</sub>O + Na<sub>2</sub>O) content ranging from 2.88% to 4.16%. The Na<sub>2</sub>O/K<sub>2</sub>O ratio was found to be between 2.56 and 3.99. The Eu anomaly was absent ( $\delta\text{Eu} = 0.91\text{--}0.95$ ), suggesting no influence of plagioclase fractionation during the rock formation process. The Ce anomaly was found to be absent ( $\delta\text{Ce} = 1.04\text{--}1.08$ ). The Mg<sup>#</sup> was found to range from approximately 40.06 to 45.06, indicating minimal crystal fractionation within the magma. The mafic dikes are enriched in light rare earth elements and large ion lithophile elements (LILE) and Th, while they showed significant depletion of high field strength elements (Nb, Ta, Ti). The Ti depletion may be related to the separation and crystallization of Ti-bearing minerals such as amphibole and ilmenite. Zr and Hf anomalies were evident, likely due to the contamination of zircon minerals in the samples. The mafic dikes were most likely products of the Middle–Late Yanshanian magmatic intrusion, formed in an extensional setting within the intracontinental rift environment caused by the collision of the Pacific Plate and the Eurasian Plate. The lithospheric mantle source was influenced by subduction zone fluid, and the magma source region exhibited mixed crustal materials.



**Citation:** Huang, Y.; Chen, X.; Xie, Y. Geochemical Characteristics and Geological Significance of the Shangsü Mafic Dikes in Jiangxi. *Minerals* **2023**, *13*, 943. <https://doi.org/10.3390/min13070943>

Academic Editor: Giorgio Garuti

Received: 2 June 2023

Revised: 11 July 2023

Accepted: 12 July 2023

Published: 14 July 2023



**Copyright:** © 2023 by the authors. Licensee MDPI, Basel, Switzerland. This article is an open access article distributed under the terms and conditions of the Creative Commons Attribution (CC BY) license (<https://creativecommons.org/licenses/by/4.0/>).

**Keywords:** mafic dikes; elemental geochemistry; Shangsü; Jiangxi

## 1. Introduction

The South China region is a vital metal mineralization area in China, characterized by complex geological and tectonic evolution. It experienced a complex tectonic evolution since the early Cambrian and further underwent the assembly and breakup of global supercontinents and the amalgamation and separation of the North and South continents [1–3]. It is an essential component of global plate tectonic evolution [4–7].

This region is China’s largest granite uranium mineralization area, and previous researchers conducted extensive research work here [8,9]. Mesozoic mantle-derived magmatism’s spatial and temporal distribution in South China is closely related to uranium mineralization [10–12]. It was always a focus and challenge of research. mafic dikes are essential carriers of mantle information and are crucial in studying regional tectonic evolution [13–16]. Accurate isotopic dating and elemental geochemical studies can determine the temporal sequence of tectonic evolution and provide constraints for lithospheric evolution. These research results are of great significance for understanding regional geological evolution. The Shangsü area in Jiangxi is located in the western segment of the “Pingxiang-Shaoxing suture zone” within the “Qinhang eastern junction zone” where the Yangtze Plate and Huaxia Plate are combined, exhibiting a complex tectonic system. The

area is situated at the junction of the Yangtze Block and the South China Fold Belt. The northern part corresponds to the western segment of the “Pingxiang-Le’an Depression”, the central part corresponds to the western segment of the “Wugongshan Uplift”, and the central-western and southern parts are part of the “Yongxin Depression”. The South China Block underwent the influence of three major tectonic systems, resulting in a superimposed and composite tectonic pattern. Due to its unique location and tectonic environment, it created favorable conditions for mineralization in the region, and previous researchers made some research achievements in this region [1,10,11,14,17–34].

Mafic dikes in the South China region received extensive research attention recently. By analyzing the formation environment of mafic dikes and their relationship with coeval granites, their impact on mineralization processes was investigated in depth [5,35–37]. In this study, samples of mafic dikes collected from Nanyuan Mountain in the Shangsū area were subjected to petrographic examination and major and trace element geochemical analysis. The aim was to investigate the origin, source characteristics, and geological significance of the mafic dikes in this region, providing valuable information for further analysis of the Mesozoic magmatic evolution and petrogenetic dynamics in the South China region.

## 2. Regional Geological Background

The Shangsū area in Jiangxi is located between the Yangtze Block and the Huaxia Block, with all exposure except the Upper Proterozoic, Lower Paleozoic, and Tertiary sediments. The traditional boundary between the Yangtze Platform and the South China Fold Belt is located south of this area, passing through the Pingle depression belt between the Jiuling and Wugong uplifts in central Jiangxi, trending northeast. The Shangsū area is located at the western end of the depression and is divided into two parts, north and south, which are connected east–west. The Middle Proterozoic Shuangqiao Formation and Devonian strata constitute an allochthonous system of thrusting and nappe structures along the southern margin of the Jiuling uplift, trending northeast. The Permian formations and Lower Triassic formations also have sporadic distributions. The Upper Triassic and Cretaceous are distributed in the central-western part of the study area, while the Quaternary is distributed in river systems and intermountain basins. The stratigraphy of the Shangsū area consists of the Neoproterozoic Shenshan Group and the Sinian metamorphic rocks, which are widely distributed. The overlying layers include the Cambrian, Devonian to Cretaceous, and Quaternary rocks. The geological evolution of the Shangsū area underwent a process of transition from oceanic to continental setting, which includes several stages. The first stage is the formation of the primitive continental crust from the Paleoproterozoic to the early Ediacaran, The second stage is the tectonic consolidation stage of the Cathaysia and Yangtze blocks during the South China Orogenic Movement, followed by the formation stage of the Wugongshan uplift from the late Ordovician to the early Silurian, the intracontinental Pingle depression stage from the late Paleozoic to the early Cretaceous, and the fault-controlled basin formation stage since the late Cretaceous. Ultimately, a three-layered structure of the uplifted basement, overlying cover basin, and fault-controlled basin was formed, with a structural pattern formed by the mutual superposition of the northeast and north-northeast-trending fault systems during the Yanshanian orogeny. The six samples of dolerite collected in this study intruded into the fine interbedded sandstone within deep gray, gray-black thin to medium-bedded mudstone and siltstone (Figure 1c).

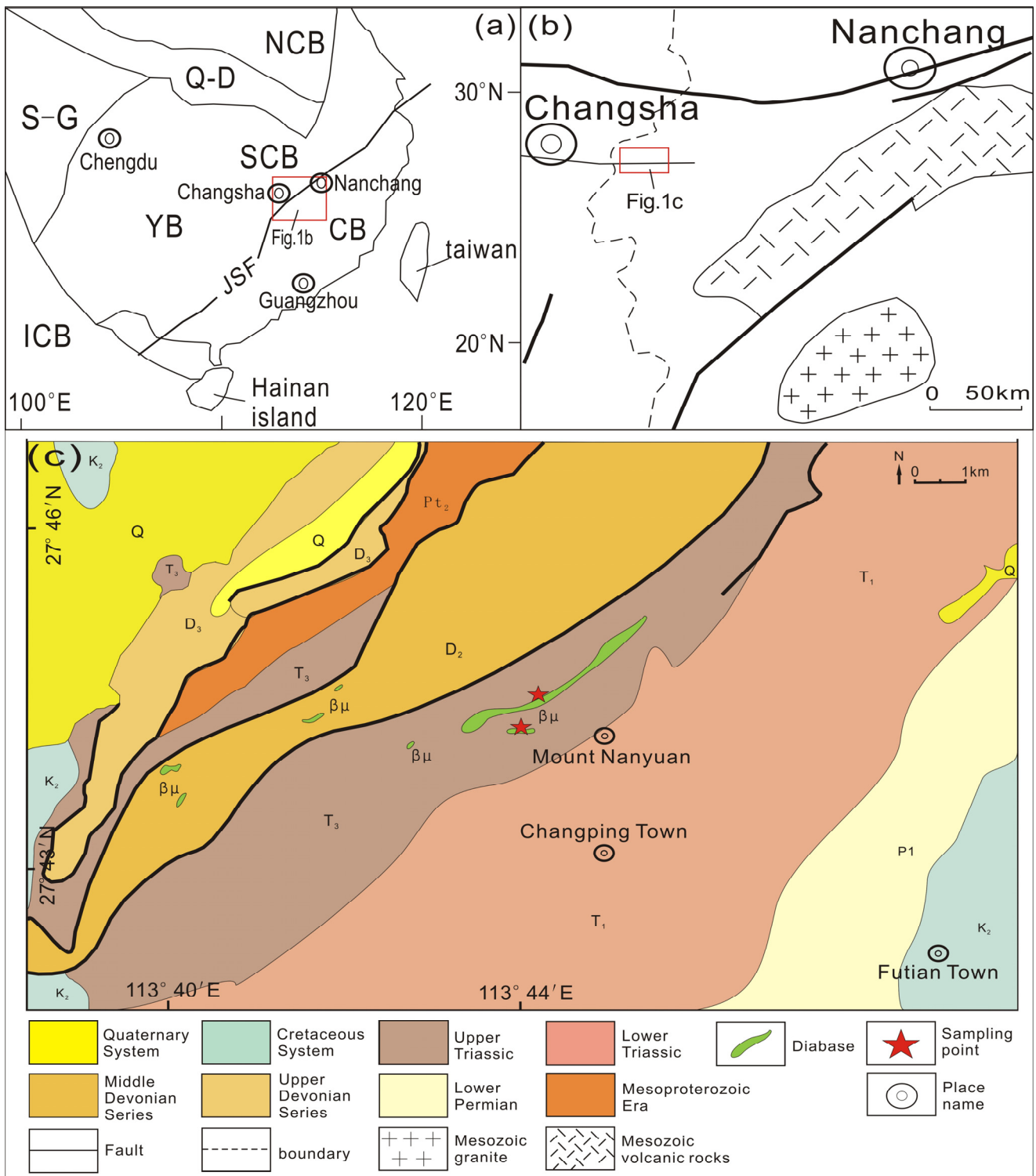


**Figure 1.** Location (a,b) and geological sketch (c) of study area. (a) Adopted from [38], (b) adopted from [39], (c) adopted from the geological map from the Jiangxi Provincial Geological Information Center.

### 3. Petrographic Characteristics of the Samples

The mafic dikes in Nanyuanshan have a width of about 100 m and extend for approximately 4500 m, with a strike direction of 320° and a dip angle of 42°. Another dike to the southwest has a width of about 70 m and extends for approximately 500 m, but

its orientation is unclear. The two mafic dikes are controlled by northeast-southwest and east-west structural fractures. The samples were taken near the middle section of Nanyuan Mountain. The dolerite rocks were dark green in color, relatively complex, exhibiting inter-growth with elongated structures, diabasic textures, and blocky textures. The polarizing microscope used was the Leica DM2500P. Thin section identification under the microscope indicated that these samples mainly comprise clinopyroxene, plagioclase feldspar, and opaque minerals. JX001 and JX002 samples contained phenocrysts. The rocks were found to be composed of clinopyroxene (39%–45%), plagioclase feldspar (54%–60%), and opaque minerals (1%). The matrix plagioclase feldspar exhibited euhedral tabular morphology with a grain size of approximately 0.3–1 mm, and plagioclase is often affected by sericitization, the plagioclase laths are located chaotically and being internally filled with xenomorphic clinopyroxene. The diameter of the internally filled xenomorphic clinopyroxene is around 0.2–0.6 mm and the plagioclase laths are located chaotically. The phenocrystic clinopyroxene exhibited subhedral to xenomorphic columnar morphology with a grain size of 1.5–4 mm with prominent projections, and with interference colors reaching a third-order orange-red. It is commonly enclosed by euhedral tabular plagioclase feldspar with a grain size of approximately 0.3–0.6 mm. Opaque minerals were found to be present in small amounts, mainly iron-bearing minerals with varying grain sizes of 0.5–1 mm (Figure 2).

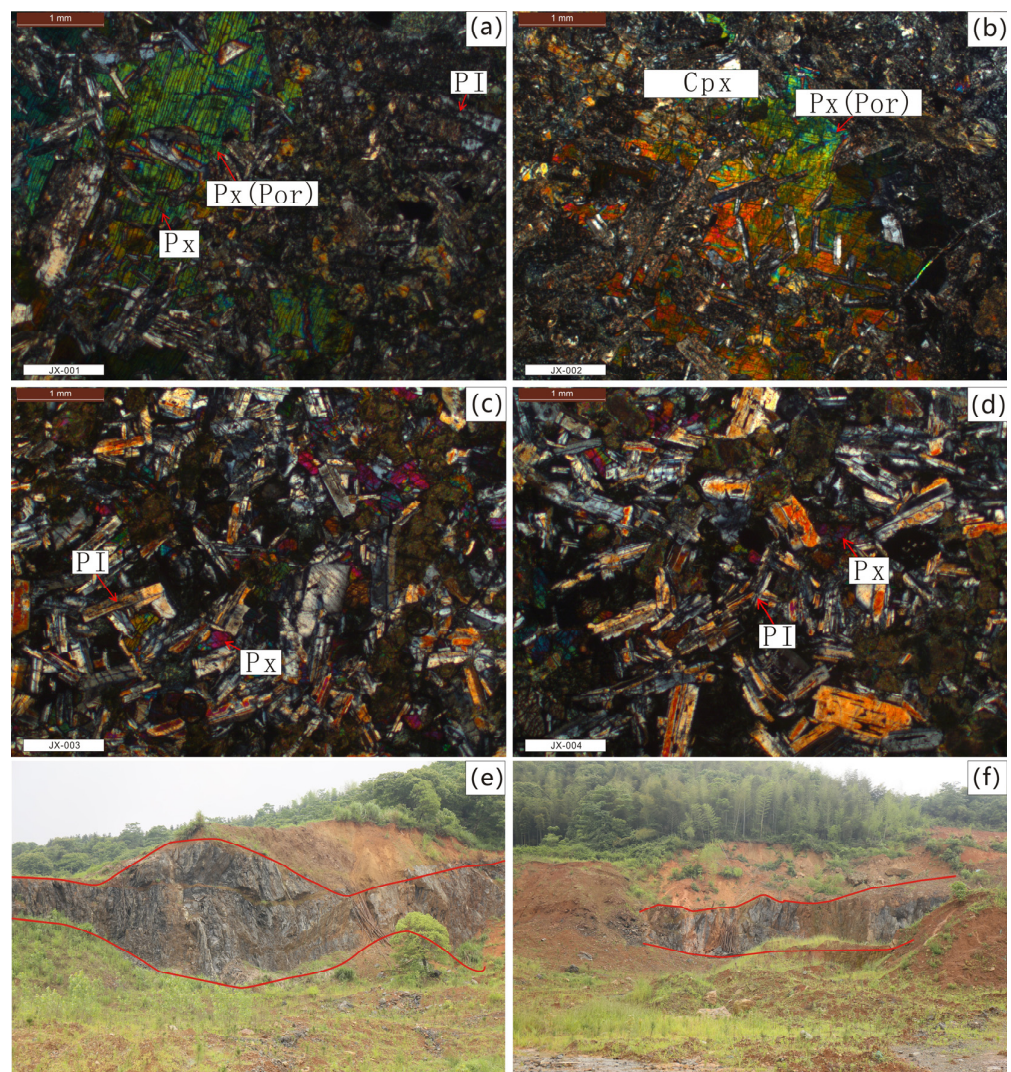


**Figure 2.** Microscopic photographs and field photographs of the mafic dikes (a–d) is the number of Microscopic photographs; (e,f) is the number of field photographs; Px: pyroxene, PI: plagioclase, CPX: clinopyroxene, Por: Porphyritic.

#### 4. Analysis Methods and Results

A total of 6 sets of samples were tested, and fresh block-like rock samples were selected from the sampling area for analysis and testing conducted by Jiangxi Jinyuan Nonferrous Geological Testing Co., Ltd. The significant elements of the rocks were determined using an X-ray fluorescence spectrometer (model: Axios mAX (I-114)), while trace elements and rare earth elements were determined using an Inductively Coupled Plasma Mass Spectrometer (model: ICP-MS-7700x (I-100)). The analysis was conducted using national standards such as methods for chemical analysis of silicate rocks: GB/T14056.28-2010 and GB/T14506.30-2010, and the accuracy was better than 5%. The analytical results are shown in Table 1.

**Table 1.** Major and trace element analyses of dolerite in the Shangsu area.

Sample ID	JX-001	JX-002	JX-003	JX-004	JX-005	JX-006
LOI *	4.17	4.42	4.11	3.49	2.87	3.63
SiO <sub>2</sub> *	50.53	49.46	48.40	48.59	49.94	48.38
Al <sub>2</sub> O <sub>3</sub> *	16.63	16.89	17.55	17.49	17.81	17.21
Fe <sub>2</sub> O <sub>3</sub> *	8.97	9.41	9.20	9.41	8.96	9.59
CaO *	6.59	6.41	9.00	9.01	8.74	8.84
MgO *	7.14	7.36	7.63	7.63	6.53	7.53
TiO <sub>2</sub> *	0.91	0.95	0.85	0.90	1.05	0.94
MnO *	0.16	0.16	0.15	0.15	0.16	0.17
P <sub>2</sub> O <sub>5</sub> *	0.11	0.12	0.10	0.11	0.13	0.12
K <sub>2</sub> O *	0.94	0.91	0.68	0.73	1.03	0.88
Na <sub>2</sub> O *	3.68	3.64	2.20	2.30	2.63	2.48
V	149	148	140	146	168	149
Cr	217	300	263	260	215	219
Co	37.0	38.7	40.2	40.7	34.0	38.2
Ni	97.2	136	121	117	73.8	107
Ga	15.8	15.3	15.7	16.5	16.5	15.4
Sr	352	330	223	212	238	226
Zr	248	1099	159	581	246	1021
Nb	7.19	7.20	5.85	6.24	7.23	6.64
Ba	382	349	166	163	253	204
Hf	6.51	27.8	4.40	15.1	6.71	26.3
Ta	0.49	0.48	0.41	0.43	0.50	0.46
Pb	13.0	13.4	8.62	9.53	10.3	7.26
Th	4.05	4.04	3.89	4.18	4.91	4.41
U	0.58	0.57	0.51	0.56	0.65	0.60
Rb	38.6	35.1	19.0	20.3	30.6	28.0
Sc	26.9	30.6	23.9	25.1	30.7	27.4
Y	31.8	89.0	27.8	56.2	37.7	86.0
La	14.0	14.5	13.3	13.4	16.4	14.9
Ce	30.1	32.0	29.5	30.5	36.4	33.4
Pr	3.56	3.66	3.42	3.56	4.19	3.84
Nd	14.4	15.2	14.1	14.9	17.4	15.8
Sm	3.30	3.43	3.29	3.39	3.98	3.53
Eu	1.07	1.10	1.10	1.11	1.27	1.13
Gd	3.66	3.98	3.72	3.92	4.57	4.09
Tb	0.66	0.69	0.65	0.67	0.80	0.71
Dy	4.18	4.41	4.33	4.51	5.24	4.81
Ho	0.95	0.99	0.95	1.01	1.17	1.06
Er	2.86	3.08	2.86	3.05	3.60	3.16
Tm	0.45	0.44	0.44	0.46	0.53	0.48
Yb	2.81	3.05	2.94	3.00	3.53	3.21
Lu	0.46	0.48	0.45	0.46	0.54	0.48
LREE/HREE	4.14	4.08	3.96	3.91	3.99	4.03
Mg <sup>#</sup>	43.28	43.34	43.91	44.91	40.06	45.06

Table 1. Cont.

Sample ID	JX-001	JX-002	JX-003	JX-004	JX-005	JX-006
$\delta\text{Eu}$	0.94	0.91	0.95	0.93	0.91	0.909
$\delta\text{Ce}$	1.04	1.07	1.07	1.08	1.07	1.08
$\text{La}_N/\text{Yb}_N$	3.57	3.41	3.25	3.20	3.33	3.33

Note: Major element concentrations have been recalculated on a dry basis. Element concentrations marked with \* are given in percentage (%), while other units are in parts per million (ppm).

### 5. Geochemical Characteristics

The analyzed samples of Shangsu mafic dikes were found to have an  $\text{SiO}_2$  content ranging from 48.38% to 50.53%, which is normal. The  $\text{MgO}$  content ranged from 6.53% to 7.63%. The  $(\text{K}_2\text{O} + \text{Na}_2\text{O})$  content ranged from 2.88% to 4.16%. The samples had a high  $\text{Na}_2\text{O}$  content with  $\text{Na}_2\text{O} > \text{K}_2\text{O}$ ; the range of  $\text{Na}_2\text{O}/\text{K}_2\text{O}$  was 2.56 to 3.99. In the  $\text{SiO}_2$ -Nb/Yb diagram (Figure 3a), the rocks belonged to the sub-alkaline basalt region. Meanwhile, in the Th/Yb-Ta/Yb diagram (Figure 3b), it was classified under the calc-alkaline series. The range of  $\text{Fe}_2\text{O}_3$  content was 8.96% to 9.59%. The  $\text{Al}_2\text{O}_3$  content was relatively high, ranging from 16.63% to 17.81%. The range of  $\text{CaO}$  content was 6.41% to 9.01%. Additionally, the samples exhibited low  $\text{TiO}_2$  content ranging from 0.91% to 1.05%, with an average of 0.94%, indicating they belonged to the low-Ti basaltic rock series. The rare earth element abundance of the mafic dikes samples from the Shangsu area was (81.03~99.71) ppm, with an average of 87.43 ppm. The range of LREE/HREE ratio was 3.91 to 4.14, with an average of 4.02. The normalized distribution pattern of chondritic meteorites exhibited a differentiated with light rare earth element enrichment and heavy rare earth element depletion (Figure 4a). The range of  $(\text{La}/\text{Yb})_N$  was 3.20 to 3.57. The differentiation degree between LREE and HREE was not significant. The range of  $(\text{La}/\text{Sm})_N$  was 2.55 to 2.74, with an average of 2.67, while the range of  $(\text{Gd}/\text{Lu})_N$  was 0.98 to 1.05, with an average of 1.03. There was no significant differentiation between light and heavy rare earth elements. The samples showed no Eu anomaly ( $\delta\text{Eu} = 0.91\sim 0.96$ , with an average of 0.93), and Ce showed no anomaly ( $\delta\text{Ce} = 1.02\sim 1.06$ , with an average of 1.05). In the primitive mantle-normalized spider diagram (Figure 4b), the samples were significantly enriched in large ion lithophile elements (such as K, Rb, Ba, Th) and LREE, while high field strength elements Nb and Ti showed significant depletion. The shape of the trace element distribution curve exhibited a left-side peak and a gentle right-side slope. Zr and Hf showed positive anomalies. The range of the Rittmann index  $\sigma$  was 1.54 to 3.20, indicating that the samples belonged to the calc-alkaline rock series.

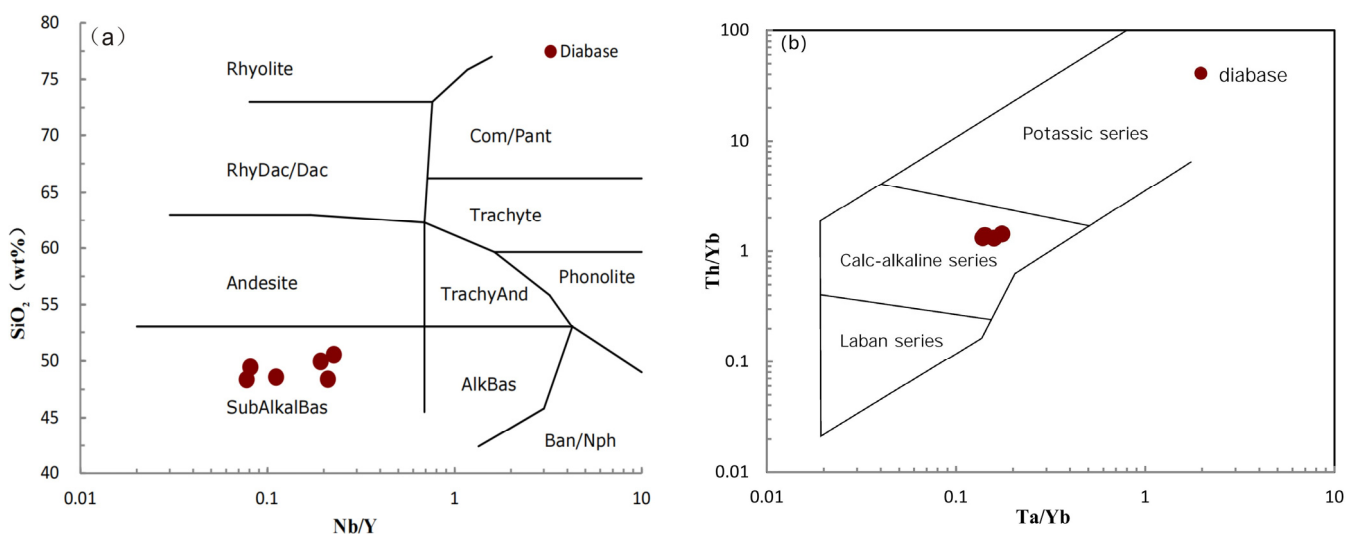
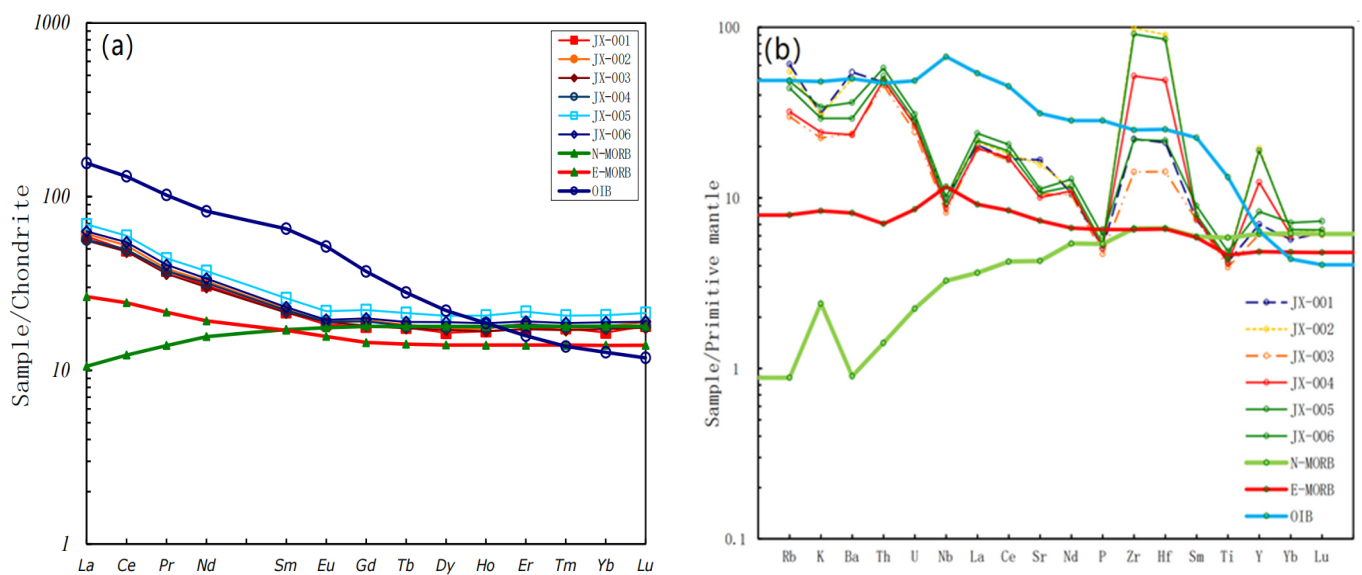


Figure 3.  $\text{SiO}_2$ -Nb/Y (a) and Th/Yb-Ta/Y (b) diagrams of the Shangsu dolerite (a) adopted from [40], (b) adopted from [41].



**Figure 4.** Primitive mantle-normalized multi-element diagram (a) and reference values for primitive mantle and chondrite, (b) reference values for MORB and chondrite adopted from [42].

## 6. Discussion

### 6.1. Nature of Magma Source Region

The samples of dolerite from the Shangsus area exhibited a variation range of ignition loss from 2.87% to 4.42%, indicating a potential late-stage alteration influence. However, the high field strength elements (such as Zr, Nb, Pb, U) and immobile elements like rare earth elements and Ti were relatively less affected, making them better indicators of the characteristics of the magma source region and the genesis of the rocks. The dolerite dikes in the Shangsus are located in the sub-alkaline basalt field in the  $\text{SiO}_2\text{-Nb/Y}$  diagram, and they are relatively enriched in large ion lithophile elements (K, Rb, Ba) and light rare earth elements. They were found to exhibit geochemical characteristics of depletion in high-field strength elements Nb, Ti, and P. The significant depletion of Nb indicates the characteristics of an island arc environment, while the depletion of Ti may be related to the separation and crystallization of Ti-bearing minerals such as ilmenite and titanomagnetite. The depletion of P suggests a low degree of apatite separation and crystallization. Th-U were higher than that of La. These facts along with negative anomalies of Nb and Ti were geochemical signatures of crustal contamination of mafic magmas. In the  $\text{TiO}_2\text{-Zr}$  diagram (Figure 5a), the samples are located in the transitional zone between intra-plate basalts and volcanic arc basalts, suggesting possible influence from fluid-metasomatized mantle source region associated with subduction-induced dehydration [43]. The samples are located in the field of intra-plate basalt in the  $\text{Zr}/4\text{-2Nb-Y}$  diagram (Figure 5b). The samples are located in the continental margin arc region in the  $\text{Th/Yb-Ta/Yb}$  diagram (Figure 5c), indicating a possible enrichment of Th due to fluid-metasomatism in the mantle source region associated with subduction-induced dehydration [43], causing the sample to deviate from its original evolutionary trend. It projects onto the field of intra-plate basalt in the  $\text{Zr/Y-Zr}$  diagram (Figure 5d). In Figure 6a, all the samples belong to the crust-mantle source type, indicating that the magmatic formation process likely involved the participation of crustal material and fluids. The dolerite was rapidly intruded during the extensional tectonic stage of plate movement in southern China, suggesting a fast magma ascent. During this rapid ascent, the degree of crustal contamination will likely be minimal [18].

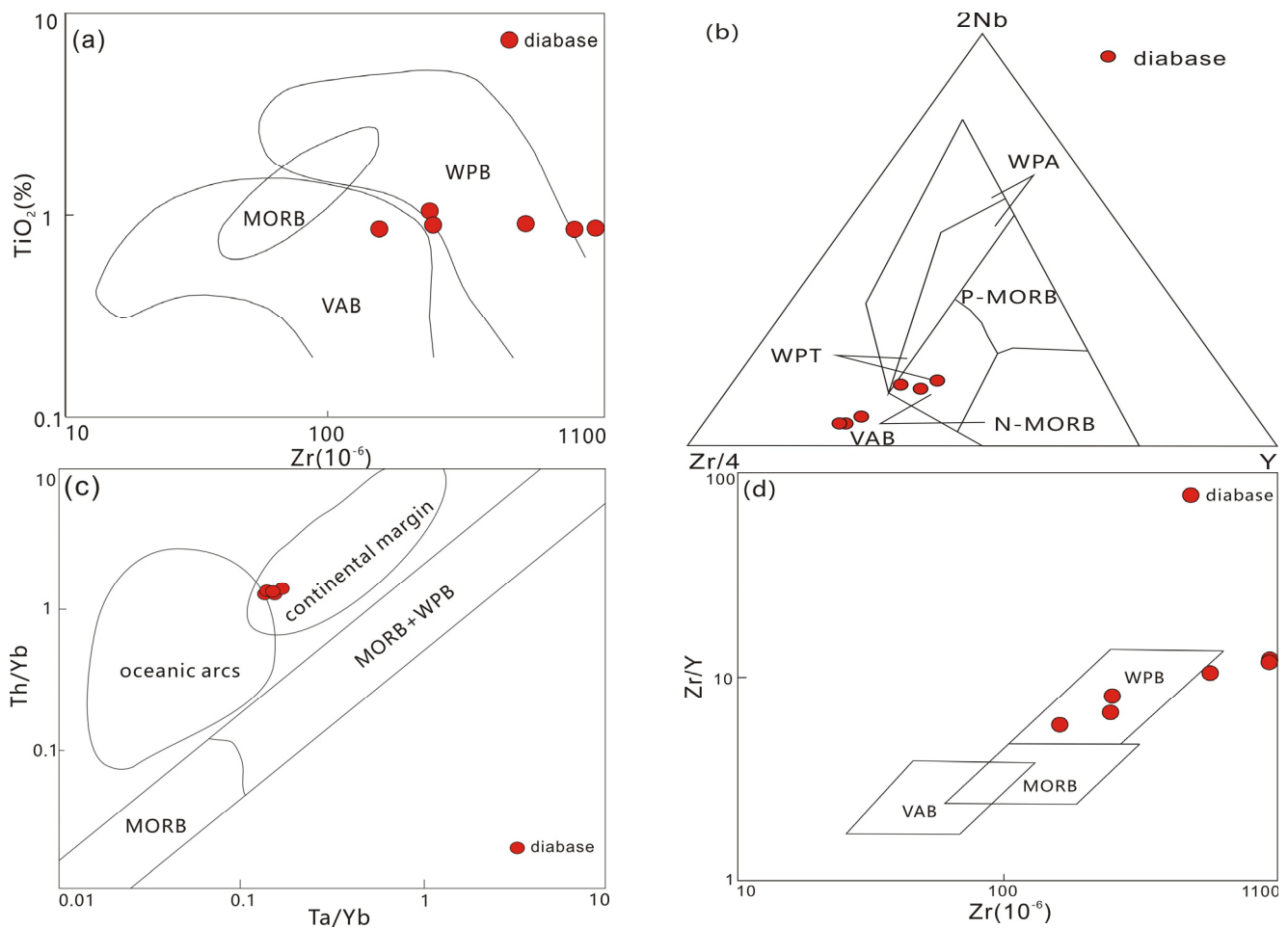


**Figure 5.** Diagrams of discrimination for the tectonic setting of the Shangsu dolerite. (a) Adopted from [41], (b) adopted from [44], (c) adopted from [45], (d) adopted from [46].

The samples in Figure 6b were located in the lithospheric mantle zone, and in Figure 7, the samples exhibited a trend of fluid-induced enrichment, indicating that the Shangsu dolerite was derived from a mantle source region enriched by subduction zone fluid. It suggests that the Shangsu dolerite is a product of fluid-rock interaction and melting in the lithospheric mantle, formed through the interaction between crustal material and dehydration of subducted slab. The enrichment in large ion lithophile elements (such as K, Rb, Ba) in the samples may be attributed to the fluids released during the phase transition of the subducted slab, carrying mobile elements such as K, Rb, Sr, and the interaction between the fluids and the overlying mantle wedge leading to the enrichment of these elements in the mantle wedge melting island arc magmas. Meanwhile, high-field strength elements do not enter the mantle wedge with water fluids, and the mantle wedge, enriched in significant ion lithophile elements, undergoes melting, resulting in high contents of LILE and relative depletion of HFSE.

The samples had relatively high Zr abundance of (159~1099) ppm, with JX-002 and JX-006 samples having Zr abundance of 1099 ppm and 1021 ppm, respectively, which was much higher than the other four samples. The high anomaly of Zr was speculated to be due to the assimilation of crustal zircon by mafic magma, with corresponding Hf abundance of 27.8 ppm and 26.3 ppm, also significantly higher than the other four samples. Together with Zr, Hf exhibited abnormally increased contents. The samples exhibited relatively high MgO contents (6.53%–7.63%), with an average value of 7.30%. The  $Mg^\#$  values ranged from 40.06 to 45.06, with an average of 43.43, lower than the original magma. The samples showed no Eu anomalies, the variation range of MgO content was 6.53%–7.63%, the variation

range of  $\text{SiO}_2$  content was 48.38%–50.53%, and the variation range of  $\text{Mg}^\#$  content was 40.06%–45.06%, indicating magma differentiation and crystallization. The  $\text{Na}_2\text{O}$  content in the samples was high, with  $\text{Na}_2\text{O} > \text{K}_2\text{O}$ . The Nb/U values ranged from 11.05 to 12.67, it was significantly lower than MORB and OIB and was located between the upper and lower crust, suggesting the presence of partial crustal material in the source region of the study area [47]. The Nb/Ta ratios ranged from 14.41 to 14.87, and the Zr/Hf ratios ranged from 36.15 to 39.55, generally consistent with the primitive mantle. The high ratios of La/Nb ( $>1.5$ ) and La/Ta ( $>28$ ) indicated characteristics of molten magma.

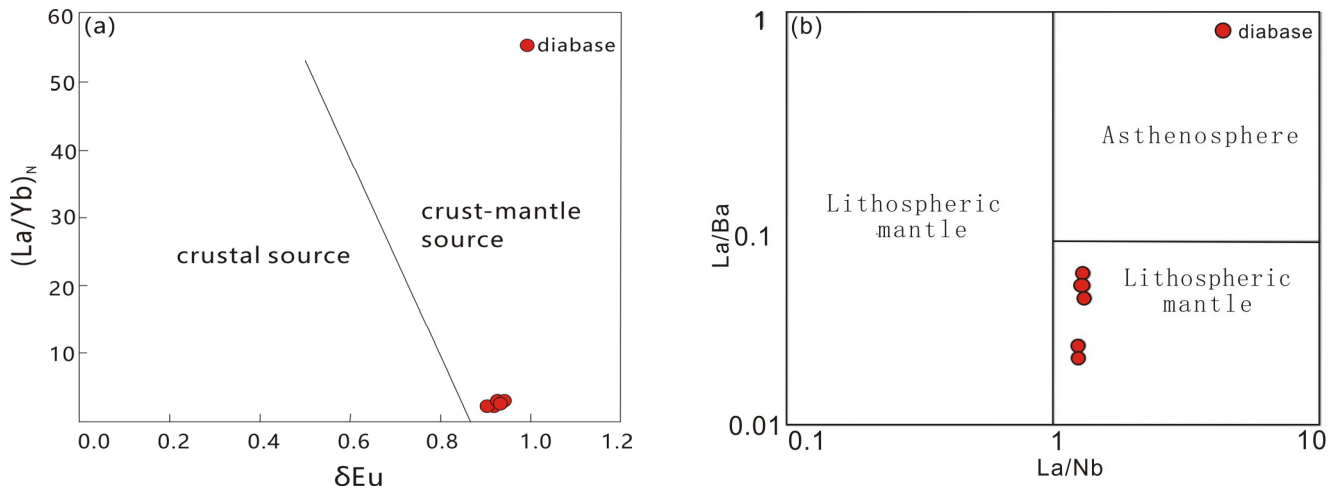


**Figure 6.**  $(\text{La}/\text{Yb})_N$ - $\delta\text{Eu}$  (a) and  $\text{La}/\text{Ba}$ - $\text{La}/\text{Nb}$  (b) diagrams of the Shangsu diabase. (a) adopted from [48], (b) adopted from [49].

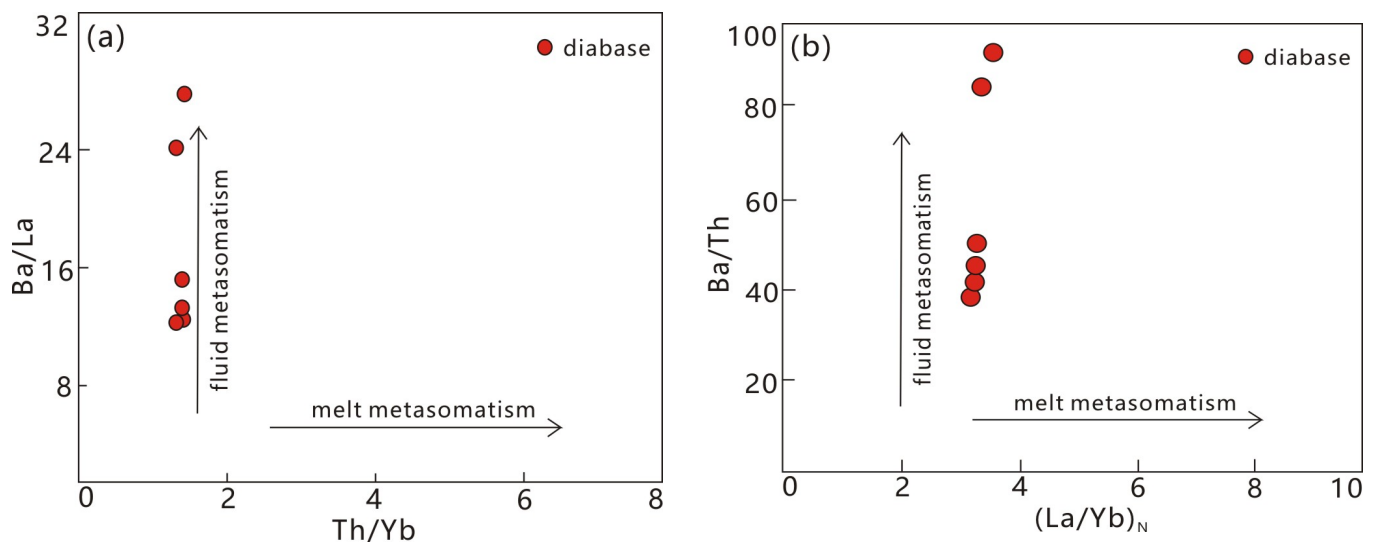


**Figure 7.**  $\text{Ba}/\text{La}$ - $\text{Th}/\text{Yb}$  (a) and  $\text{Ba}/\text{Th}$ - $(\text{La}/\text{Yb})_N$  (b) diagrams of Shangsu diabase. Adopted from [48].

## 6.2. Tectonic Background

The Mesozoic magmatic activity in the South China region was widespread [14,23,50]. Researchers believe that during the Early Cretaceous, the tectonic pattern in South China transitioned from compression and uplift to extensional rifting. During this period, asthenospheric upwelling and lithospheric extension formed a series of mafic dikes, which exhibited characteristics of intra-plate basalt [35,43,51]. Most scholars believe that the multiple episodes of magmatic activity during the Jurassic to Cretaceous in an extensional setting

were a response to the westward subduction of the Pacific Plate beneath the Eurasian continental plate [4,6,9,12,25,52]. According to the 1:50,000 geological map and explanatory notes of the study area, it is evident that the Late Triassic Anyuan Formation was intruded by dolerite dikes in the Shangsu region, which are products of the Late to Middle Yanshanian magmatic intrusion activity. This period coincided with the Pacific Plate's reverse subduction and the continental lithosphere's extensional thinning [9].

Additionally, according to research conducted by other scholars in the surrounding areas, the formation of basaltic dikes in Aikou, Dean County, occurred around 120 million years ago [18]. The U-Pb age of the Yingshan deposit in Dexing was determined to be  $152 \pm 10$  million years [53]. The  $^{39}\text{Ar}$ - $^{40}\text{Ar}$  age of the Huangsha dolerite was determined to be 140 million years [54]. The U-Pb age of the Nancheng diabase in southern-central Jiangxi was determined to be  $158.0 \text{ Ma} \pm 3.4 \text{ Ma}$  [55]. Therefore, it can be inferred that the age of the Shangsu dolerite is around 150 million years, and it is a product of the Late to Middle Yanshanian magmatic intrusion activity. It formed in a tectonic setting characterized by an extensional environment due to the Pacific Plate subduction-induced lithospheric extension and thinning. The melting of the enriched mantle in the lithosphere occurred through fluid metasomatism resulting from the dehydration of the subducted slab.

## 7. Conclusions

(1) The Shangsu dolerite in the study area is a product of melting in the lithospheric mantle due to fluid metasomatism derived from the subducted slab, with evidence of crustal material mixing in the magma source.

(2) The mafic dikes distributed in the Shangsu area exhibited geochemical characteristics of intra-plate basalt. The lithospheric mantle source was influenced by subduction zone fluid. These mafic dikes are likely products of Late to Middle Yanshanian magmatic intrusion activity, formed in an intra-plate extensional environment resulting from the collision between the Pacific Plate and the Eurasian Plate.

**Author Contributions:** Fieldwork, Y.X. and X.C.; software, Y.H.; resources, X.C.; writing—review and editing, Y.H. All authors have read and agreed to the published version of the manuscript.

**Funding:** This research received no external funding.

**Data Availability Statement:** The data underlying this article are available in the article.

**Conflicts of Interest:** The authors declare no conflict of interest.

## References

1. Zhao, G.; Cawood, P.A. Precambrian geology of China. *Precambrian Res.* **2012**, *222*–223, 13–54. [[CrossRef](#)]
2. Charvet, J.; Shu, L.; Faure, M.; Choulet, F.; Wang, B.; Lu, H.; Le Breton, N. Structural development of the Lower Paleozoic belt of South China: Genesis of an intracontinental orogen. *J. Asian Earth Sci.* **2010**, *39*, 309–330. [[CrossRef](#)]
3. Charvet, J.; Shu, L.; Shi, Y.; Guo, L.; Faure, M. The building of south China: Collision of Yangzi and Cathaysia blocks, problems and tentative answers. *J. Asian Earth Sci.* **1996**, *13*, 3–5. [[CrossRef](#)]
4. Li, C.; Wang, Z.; Lü, Q.; Tan, Y.; Li, L.; Tao, T. Mesozoic tectonic evolution of the eastern South China Block: A review on the synthesis of the regional deformation and magmatism. *Ore Geol. Rev.* **2021**, *131*, 104028. [[CrossRef](#)]
5. Luo, J.C.; Qi, Y.Q.; Wang, L.X.; Chen, Y.W.; Tian, J.J.; Shi, S.H. Ar-Ar dating of mafic dykes from the Xiazhuang uranium ore field in northern Guangdong, South China: A reevaluation of the role of mafic dyke in uranium mineralization. *Acta Petrol. Sin.* **2019**, *35*, 2660–2678. [[CrossRef](#)]
6. Zhang, Y.; Dong, S. East asia multi-plate convergence in late mesozoic and the development of continental tectonic systems. *J. Geomech.* **2019**, *25*, 613–641. [[CrossRef](#)]
7. Zhang, Y.Q.; Dong, S.W.; Li, J.H.; Cui, J.J.; Shi, W.; Su, J.B.; Li, Y. The New Progress in the Study of Mesozoic Tectonics of South China. *Acta Geosci. Sin.* **2012**, *33*, 257–279. [[CrossRef](#)]
8. Jiang, W.; Shao, S.; Lin, K.; Li, H. Characteristics of granites and their geological role in uranium mineralization in South China. *World Nucl. Geosci.* **2021**, *38*, 446–456. [[CrossRef](#)]
9. Yu, X.; Chen, Z.; Hu, J.; Liu, M.; He, Y.; Peng, F. Early Cretaceous extension in South China: Constraints from east–west-trending A-type granite belts and growth strata in terrigenous basins. *Int. Geol. Rev.* **2022**, *64*, 799–819. [[CrossRef](#)]

10. Zeng, R.; Pan, J.Y.; Su, H.; Gan, D.; Zhong, F.; Du, H.; Yan, J.; Zhang, C. Geochronology and genetic mineralogy of apatite and zircon from the Huichang pyroxene diorite in southern Jiangxi Province: Implications for uranium mineralization. *Earth Sci.* **2022**, *1*, 1–45.
11. Chen, Y.; Wang, D.; Xu, Z.; Huang, F. Outline of regional metallogeny of ore deposits associated with the Mesozoic magmatism in South China. *Geotecton. Metallog.* **2014**, *38*, 219–229. [[CrossRef](#)]
12. Zhang, D.; Zhao, K.D.; Chen, W.; Jiang, S.Y. Early Jurassic mafic dykes from the Aigao uranium ore deposit in South China: Geochronology, petrogenesis and relationship with uranium mineralization. *Lithos* **2018**, *308*, 118–133. [[CrossRef](#)]
13. Halls, H.C. The importance and potential of mafic dyke swarms in studies of geodynamic processes. *Geosci. Can.* **1982**, *9*, 145–154. Available online: <https://www.researchgate.net/publication/285020850> (accessed on 10 October 2022).
14. Shu, L.S. An analysis of principal features of tectonic evolution in South China Block. Geological Bulletin of China. *Geol. Bull. China* **2012**, *31*, 1035–1053. [[CrossRef](#)]
15. Gan, C.; Wang, Y.; Zhang, Y.; Chen, X. Late Jurassic magmatism in the interior South China Block and its implication. *J. Geol. Soc.* **2019**, *176*, 737–754. [[CrossRef](#)]
16. Wang, T.; Huang, C.; Du, G.; Liu, Y.; Xie, J.; Li, H. Geochronology, geochemistry and zircon Hf-isotopes of the early Mesoproterozoic Yaopengzi dolerite in SW Yangtze block (Sichuan, SW China): Implications for the Columbia supercontinent breakup. *Geosci. J.* **2019**, *23*, 557–573. [[CrossRef](#)]
17. Ren, J. On the Geotectonics of Southern China. *Acta Geol. Sin.-Engl. Ed.* **1991**, *4*, 111–130. [[CrossRef](#)]
18. Xie, G.Q.; Hu, R.Z.; Jia, D.C. Geological and geochemical characteristics and its significance of mafic dikes from Northwest Jiangxi Province. *Geochimica* **2002**, *31*, 329–337. [[CrossRef](#)]
19. Yu, X.Q.; Wu, G.G.; Shu, L.S.; Yan, T.Z.; Di, Y.J. The Cretaceous tectonism of the Gan-Hang Tectonic Belt, southeastern China. *Earth Sci. Front.* **2006**, *13*, 31–43. [[CrossRef](#)]
20. Xie, G.Q. Late Mesozoic and Cenozoic Mafic Dikes (Bodies) from Southeastern China: Geological and Geochemical Characteristics and Its Geodynamics—A Case of Jiangxi Province. Doctoral Dissertation, Institute of Geochemistry, Chinese Academy of Sciences, Guiyang, China, 2003. Available online: <http://ir.gyig.ac.cn/handle/352002/3650> (accessed on 11 July 2023).
21. Qi, Y.; Hu, R.; Liu, S.; Coulson, I.M.; Qi, H.; Tian, J.; Feng, C.; Wang, T. Geochemical and Sr–Nd–Pb isotopic compositions of Mesozoic mafic dikes from the Gan-Hang tectonic belt, South China: Petrogenesis and geodynamic significance. *Int. Geol. Rev.* **2012**, *54*, 920–939. [[CrossRef](#)]
22. Mao, J.; Cheng, Y.; Chen, M. Major types and time-space distribution of Mesozoic ore deposits in South China and their geodynamic settings. *Miner. Depos.* **2013**, *48*, 267–294. [[CrossRef](#)]
23. Gan, C.; Wang, Y.; Zhang, Y.; Zhang, J. The earliest Jurassic A-type granite in the Nanling Range of southeastern South China: Petrogenesis and geological implications. *Int. Geol. Rev.* **2017**, *59*, 274–292. [[CrossRef](#)]
24. Xu, X.; Liang, C.; Chen, J.; Xu, Y. Fundamental geological features and metallogenic geological backgrounds of Nanling tectonic belt. *Earth Sci.* **2021**, *46*, 1133–1150. [[CrossRef](#)]
25. Yan, Q.-H.; Wang, H.; Wu, Y.; Chi, G. Simultaneous development of arc-like and OIB-like mafic dikes in eastern Guangdong, SE China: Implications for late Jurassic—Early Cretaceous tectonic setting and deep geodynamic processes of South China. *Lithos* **2021**, *388–389*, 106021. [[CrossRef](#)]
26. Mao, J.; Li, Z.; Ye, H. Mesozoic tectono-magmatic activities in South China: Retrospect and prospect. *Earth Sci.* **2014**, *57*, 2853–2877. [[CrossRef](#)]
27. Zhang, G.; Guo, A.; Wang, Y.; Li, S.; Dong, Y.; Liu, S.; He, D.; Cheng, S.; Lu, R.; Yao, A. Tectonics of South China Continent and its implications. *Earth Sci.* **2013**, *56*, 1804–1828. [[CrossRef](#)]
28. Wang, Y.; Fan, W.; Zhang, G.; Zhang, Y. Phanerozoic tectonics of the South China Block: Key observations and controversies. *Gondwana Res.* **2013**, *23*, 1273–1305. [[CrossRef](#)]
29. Ou, Q.; Lai, J.Q.; Carvalho, B.B.; Zi, F.; Kong, H.; Li, B.; Jiang, Z.Q. Different response to middle-Palaeozoic magmatism during intracontinental orogenic processes: Evidence from southeastern South China Block. *Int. Geol. Rev.* **2019**, *61*, 1504–1521. [[CrossRef](#)]
30. Liu, X.; Wang, Q.; Ma, L.; Wyman, D.A.; Zhou, J.S. Petrogenesis of Late Jurassic Pb–Zn mineralized high  $\delta^{18}\text{O}$  granodiorites in the western Nanling Range, South China. *J. Asian Earth Sci.* **2020**, *192*, 104236. [[CrossRef](#)]
31. Peng, J.; Wang, C.; Li, Y.; Hu, A.; Lu, Y.; Chen, X. Geochemical characteristics and Sm–Nd geochronology of scheelite in the Baojinshan ore district, central Hunan. *Acta Petrol. Sin.* **2022**, *37*, 665–682. [[CrossRef](#)]
32. Quan, O.; Lai, J.Q.; Carvalho, B.B.; Zi, F.; Liu, Y.Z. Early Silurian granitic rocks and associated enclaves as evidence of rapid cooling in a cognate magma system: The case of the Xuehuading–Panshanhong pluton, South China Block. *Geol. Mag.* **2020**, *158*, 1173–1193. [[CrossRef](#)]
33. Li, L.; Liao, Z.; Lei, L.; Lash, G.G.; Chen, A.; Tan, X. On the negative carbon isotope excursion across the Wuchiapingian–Changhsingian transition: A regional event in the lower Yangtze region, South China? *Palaeogeogr. Palaeoclimatol. Palaeoecol.* **2019**, *540*, 109501. [[CrossRef](#)]
34. Zhan, Y.; Shao, Y.; Liu, Q.; Zhang, X.; Chen, M.; Lu, Y.; Zhang, Y.; Tan, H. Hydrothermal rutile U–Pb dating of gold mineralization in the Jiangnan Orogen: A case study of the Hengjiangchong gold deposit in northeastern Hunan. *Ore Geol. Rev.* **2022**, *149*, 105115. [[CrossRef](#)]
35. Li, X.H.; Hu, R.Z.; Rao, B. Geochronology and geochemistry of Cretaceous mafic rocks from northern Guangdong Province, SE China. *Geochimica* **1997**, *26*, 14–31. [[CrossRef](#)]

36. Zhu, Q.; Ji, G.; Zhao, X.; Zhang, C.; Shu, X.; Hong, W. Petrogenesis of the late Mesozoic Lingshang ultramafic intrusion in northern Jiangxi Province: Chronologic and geochemical constraints. *Geol. China* **2020**, *47*, 1092–1108.
37. Lei, Z.L. Genesis and Source Lithology of Late Mesozoic Mafic Dikes in Southeastern China. Master's Thesis, Nanjing University, Nanjing, China, 2020. [[CrossRef](#)]
38. Liang, X.Q.; Li, X.H.; Qiu, Y.X. Indosinian collisional orogeny: Evidence from structural and sedimentary geology in Shiwandashan Basin, South China. *Geotecton. Metallog.* **2005**, *29*, 99–112. [[CrossRef](#)]
39. Hu, R.Z.; Bi, X.W.; Zhou, M.F.; Peng, J.T.; Su, W.C.; Liu, S.; Qi, H.W. Uranium Metallogenesis in South China and Its Relationship to Crustal Extension during the Cretaceous to Tertiary. *Econ. Geol.* **2008**, *103*, 583–598. [[CrossRef](#)]
40. Winchester, J.A.; Floyd, P.A. Geochemical discrimination of different magma series and their differentiation products using immobile elements. *Chem. Geol.* **1977**, *20*, 325–343. [[CrossRef](#)]
41. Pearce, J.A. Trace Element Characteristics of Lavas from Destructive Plate Boundaries. In *Andesites: Orogenic Andesites and Related Rocks*; Thorpe, R.S., Ed.; John Wiley and Sons: Chichester, UK, 1982; Volume 8, pp. 525–548.
42. Sun, S.S.; McDonough, W.F. Chemical and isotopic systematics of ocean basalts: Implications for mantle composition and processes, in *Magmatism in the Ocean Basins. Geol. Soc. Lond. Spec. Publ.* **1989**, *423*, 13–345. [[CrossRef](#)]
43. Li, X.H. Geochemical characteristics of Cretaceous mafic dikes from northern Guangdong, SE China: Petrogenesis, mantle sources and tectonic significance. In *Proceedings of the Mantle Dynamics and Plate Interactions in East Asia Geodynamics*, San Francisco, CA, USA, 1 December 1995. [[CrossRef](#)]
44. Meschede, M. A method of discriminating between different types of mid-ocean ridge basalts and continental tholeiites with the Nb-Zr-Y diagram. *Chem. Geol.* **1986**, *56*, 207–218. [[CrossRef](#)]
45. Pearce, J.A. Role of the sub-continental lithosphere in magma genesis at active continental margins. In *Continental Basalts and Mantle Xenoliths*; American Geophysical Union: Washington, DC, USA, 1983; Volume 1, pp. 230–249.
46. Pearce, J.A.; Norry, M.J. Petrogenetic implications of Ti, Zr, Y, and Nb variations in volcanic rocks. *Contrib. Mineral. Petrol.* **1979**, *69*, 33–47. [[CrossRef](#)]
47. Rudnick, R.L.; Shan, G. Composition of the Continental Crust. *Treatise Geochem.* **2003**, *3*, 1–64. [[CrossRef](#)]
48. Zhang, Y.; Zhong, F.; Pan, J.; Xia, F.; Qi, J.; Li, H.; Liu, W. Petrogenesis and Its Relationship with Uranium Mineralization of Diabase in Huangsha Uranium Ore-Field, South Jiangxi Province. *Earth Sci.* **2021**, *47*, 206–223. [[CrossRef](#)]
49. Fitton, J.G.; James, D.; Leeman, W.P. Basic magmatism associated with Late Cenozoic extension in the western United States: Compositional variations in space and time. *J. Geophys. Res. Solid Earth* **1991**, *96*, 13693–13711. [[CrossRef](#)]
50. Xu, Z.; Cheng, R.; He, Y.; Wang, L.; Lan, Y. Zircon U-Pb Ages, Sr-Nd Isotopes and Geological Significance of Early Jurassic Volcanic Rocks from Southwest Fujian. *Earth Sci.* **2019**, *44*, 1371–1388. [[CrossRef](#)]
51. Qi, Y.; Hu, R.; Liu, S.; Qi, H. Geochemical Characteristics of the Mafic Dikes from the Gan-Hang Tectonic Belt. *J. Jilin Univ.* **2008**, *38*, 784–794. [[CrossRef](#)]
52. Wang, L.-X.; Chang, Q.; Zhong, X.; Michael, A.W.; Zhang, C.; Yu, F. Early Jurassic mafic dykes from the Xiazhuang ore district (South China): Implications for tectonic evolution and uranium metallogenesis. *Lithos Int. J. Mineral. Petrol. Geochem.* **2015**, *239*, 71–85. [[CrossRef](#)]
53. Zhang, M.; Li, X.; Wei, X.; Mao, W.; Zhang, Z.; Tang, Y. Zircon LA-ICP-MS U-Pb Ages of diabase from Yinshan Deposit and Its Geological Significance, Dexing, Jiangxi Province, South China. *Acta Mineralogica Sin.* **2016**, *36*, 25–33. [[CrossRef](#)]
54. Nie, B.; Zhang, W.L. Ar-Ar age of the diabase and its relationship with uranium mineralization in Huangsha mining district, southern Jiangxi Province. *Miner. Resour. Geol.* **2018**, *32*, 784–794. [[CrossRef](#)]
55. Hua, C.; Yang, Q.; Zhou, W.; Guo, F. Zircon LA-ICPMS chronology and petrogeochemical characteristics of diabase in nancheng area, central Jiangxi province. *Miner. Petrol.* **2019**, *39*, 58–69. [[CrossRef](#)]

**Disclaimer/Publisher's Note:** The statements, opinions and data contained in all publications are solely those of the individual author(s) and contributor(s) and not of MDPI and/or the editor(s). MDPI and/or the editor(s) disclaim responsibility for any injury to people or property resulting from any ideas, methods, instructions or products referred to in the content.